Redox-active zeolitic transition metal oxides based on ε-Keggin units for selective oxidation

Zhenxin Zhang, [a*] Satoshi Ishikawa, [b] Qianqian Zhu, [a] Toru Murayama, [c] Masahiro Sadakane, [d] Michikazu Hara, [e] and Wataru Ueda [b*]

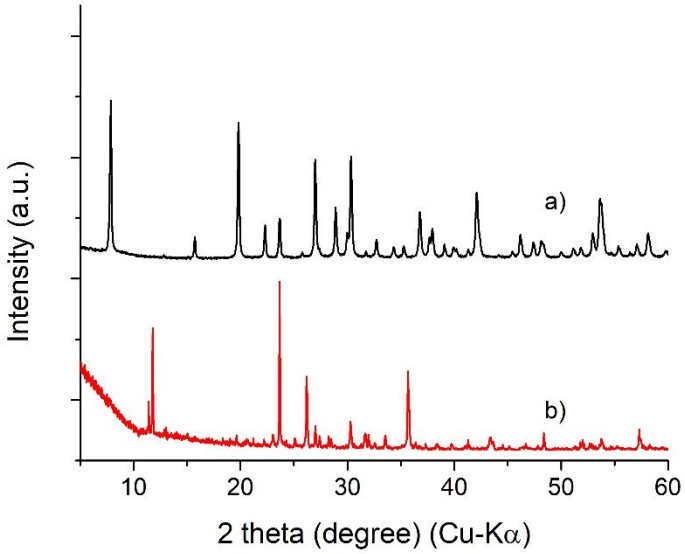

Figure S1. XRD patterns of a) **$MoFe_{0.22}O$** and b) **$MoFe_{0.22}O$** synthesized without reducing agent.

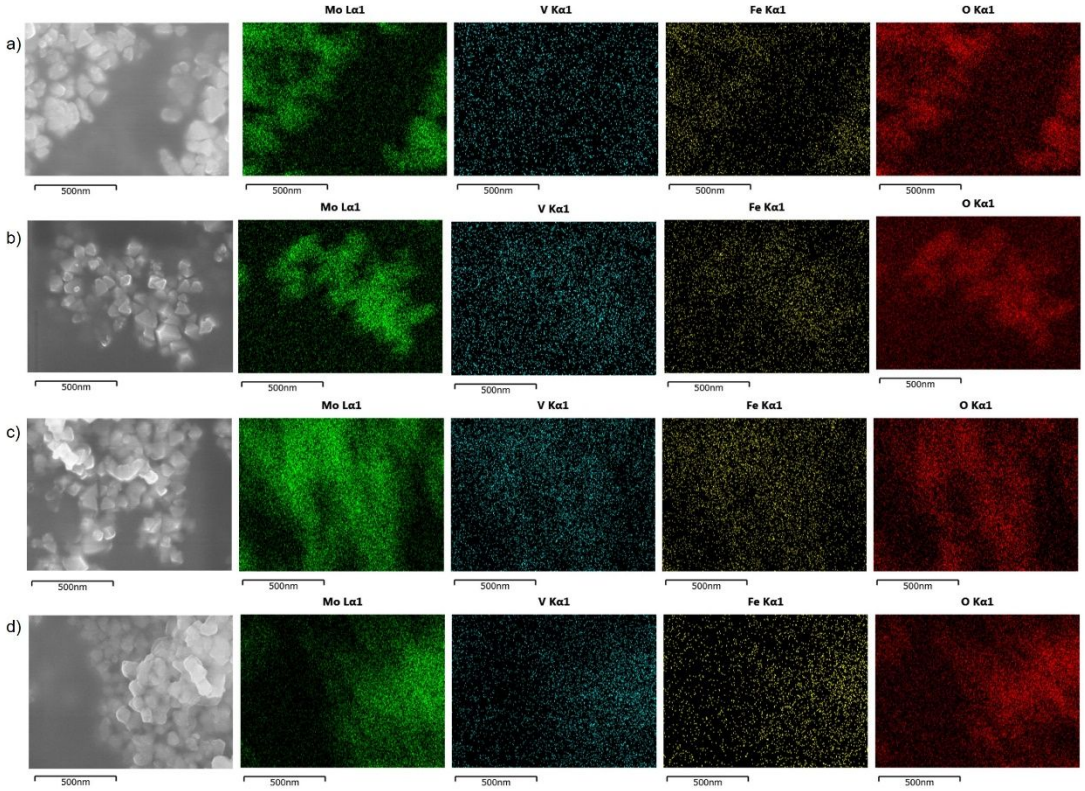

Figure S2. SEM-EDX mapping of a) $\mathbf{MoFe_{0.22}O}$, b) $\mathbf{MoFe_{0.17}V_{0.07}O}$, c) $\mathbf{MoFe_{0.14}V_{0.12}O}$, and d) $\mathbf{MoFe_{0.11}V_{0.18}O}$.

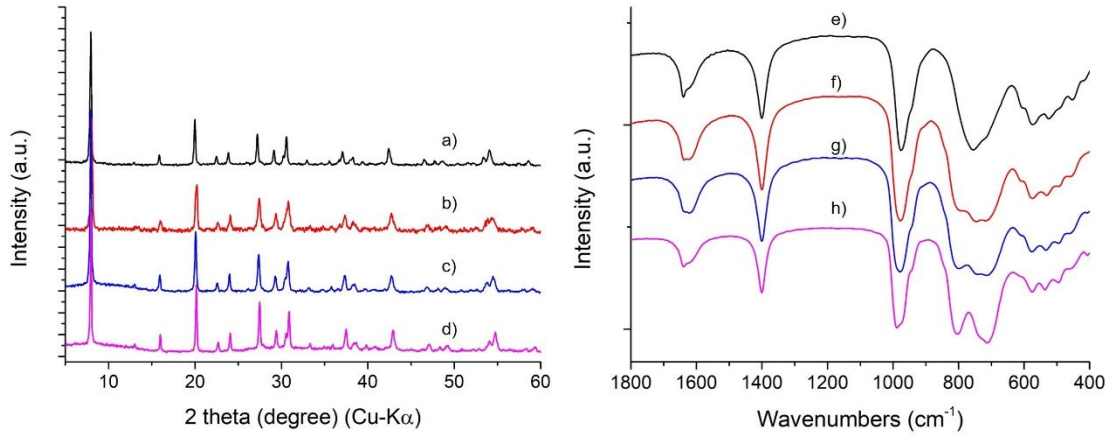

Figure S3. XRD patterns of a) **$MoFe_{0.22}O$**, b) **$MoFe_{0.17}V_{0.07}O$**, c) **$MoFe_{0.14}V_{0.12}O$**, d) **$MoFe_{0.11}V_{0.18}O$**, FTIR spectra of e) **$MoFe_{0.22}O$**, f) **$MoFe_{0.17}V_{0.07}O$**, g) **$MoFe_{0.14}V_{0.12}O$**, and h) **$MoFe_{0.11}V_{0.18}O$**.

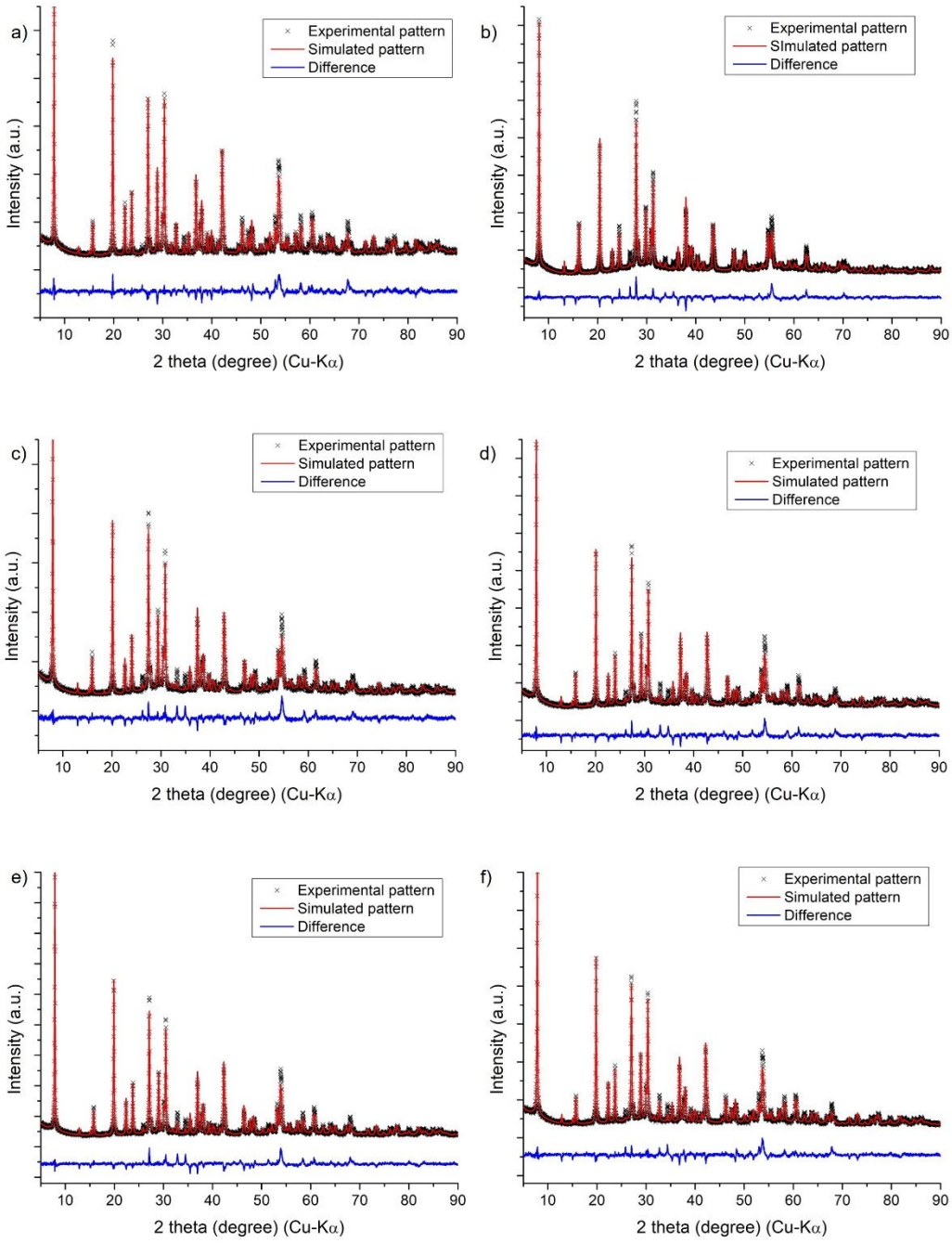

Figure S4. Comparison of simulated XRD pattern from Rietveld refinement with the experimental pattern a) **$MoFe_{0.22}O$**, b) **$MoFe_{0.22}$OAC150**, and reduction of **$MoFe_{0.22}$OAC150** with $N_2H_6SO_4$ for c) 1 h, d) 3 h, e) 9 h, and f) 20 h.

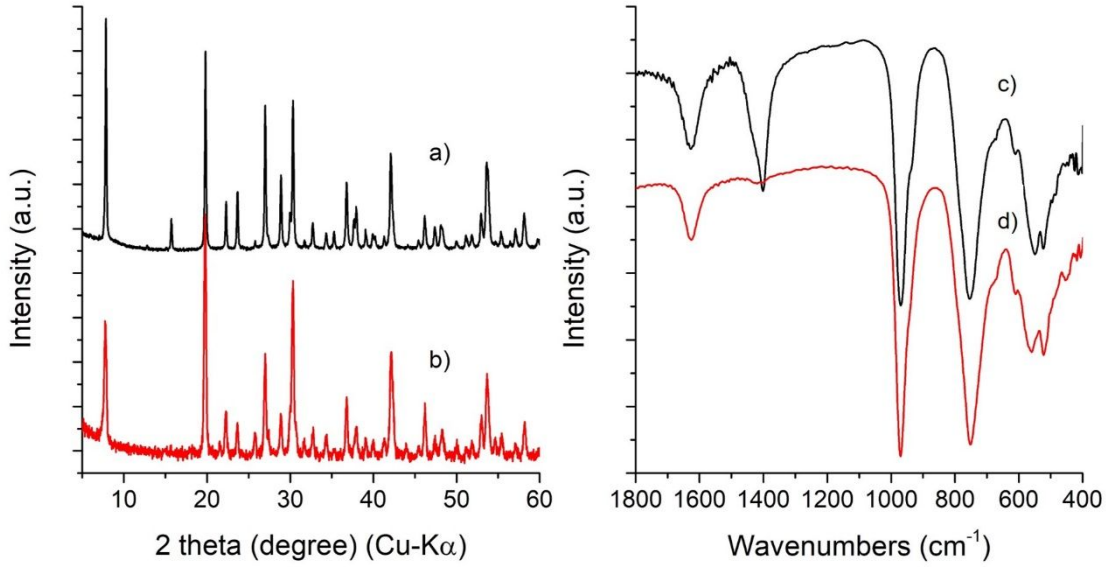

Figure S5. XRD patterns of a) **$MoFe_{0.22}O$** and b) **$CsMoFe_{0.22}O$** and FTIR spectra of c) **$MoFe_{0.22}O$** and d) **$CsMoFe_{0.22}O$**.

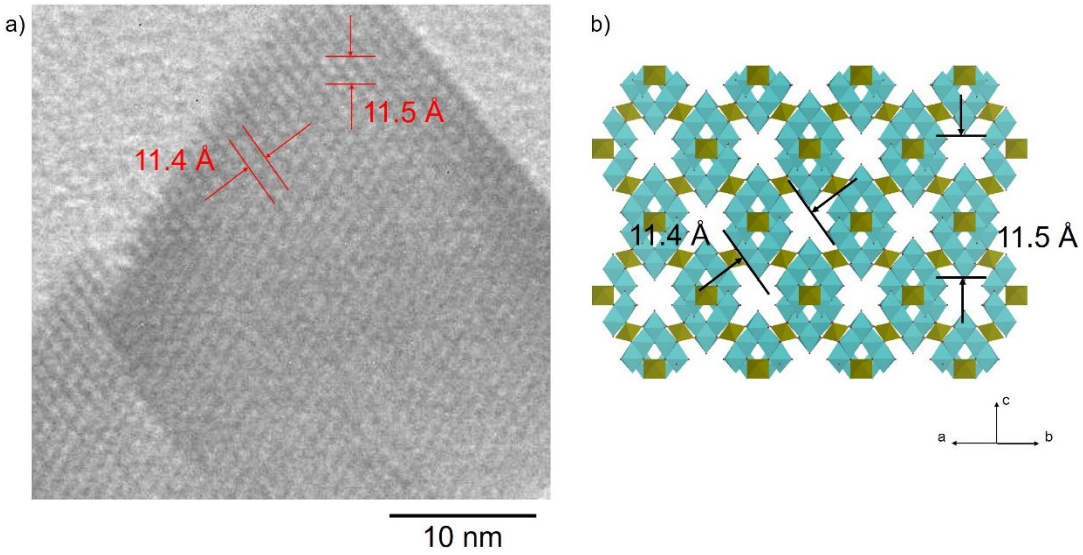

Figure S6. a) TEM image and b) structure representation of **$MoFe_{0.22}O$.**

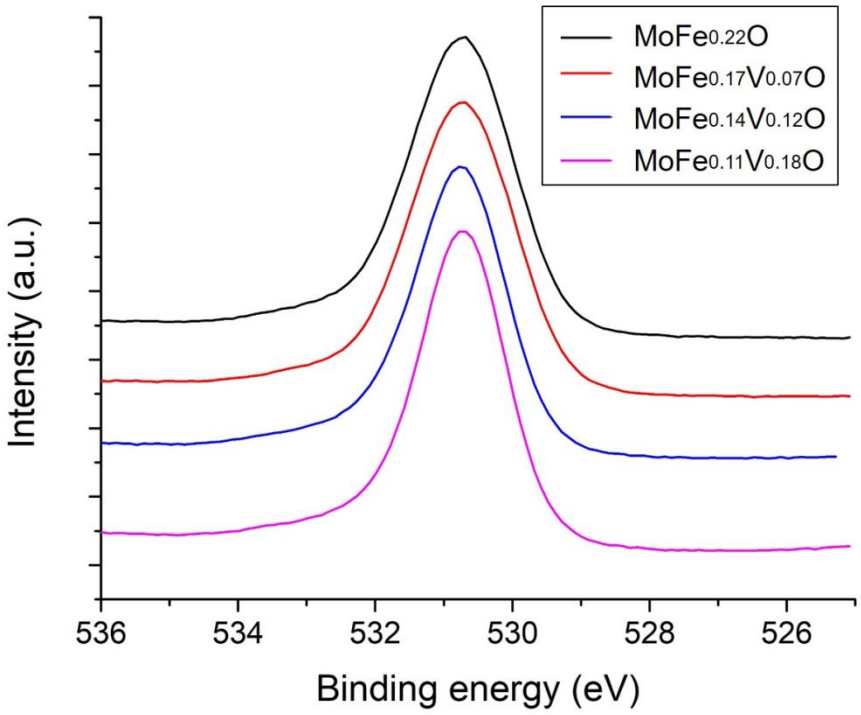

Figure S 7. XPS profiles of O(1s) of the materials

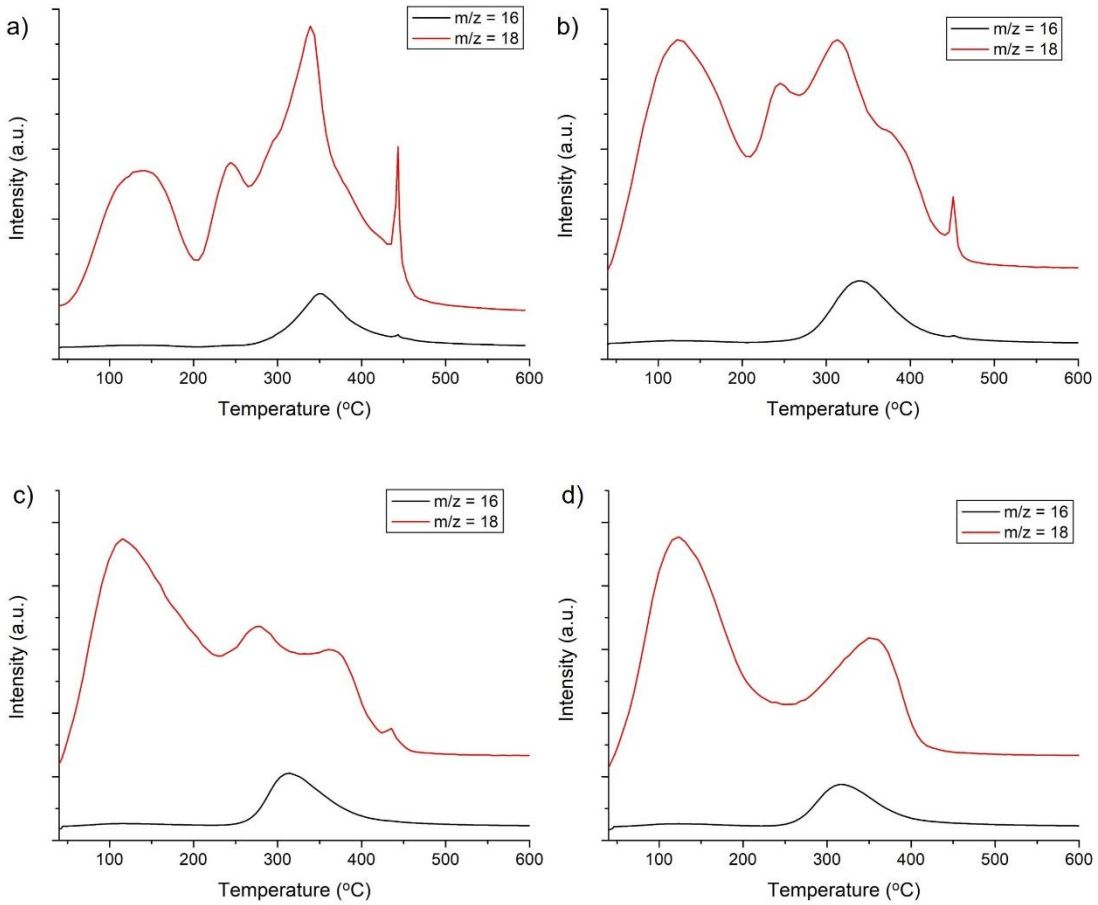

Figure S8. TPD-MS profiles of a) **$MoFe_{0.22}O$**, b) **$MoFe_{0.17}V_{0.07}O$**, c) **$MoFe_{0.14}V_{0.12}O$**, and d) **$MoFe_{0.11}V_{0.18}O$**.

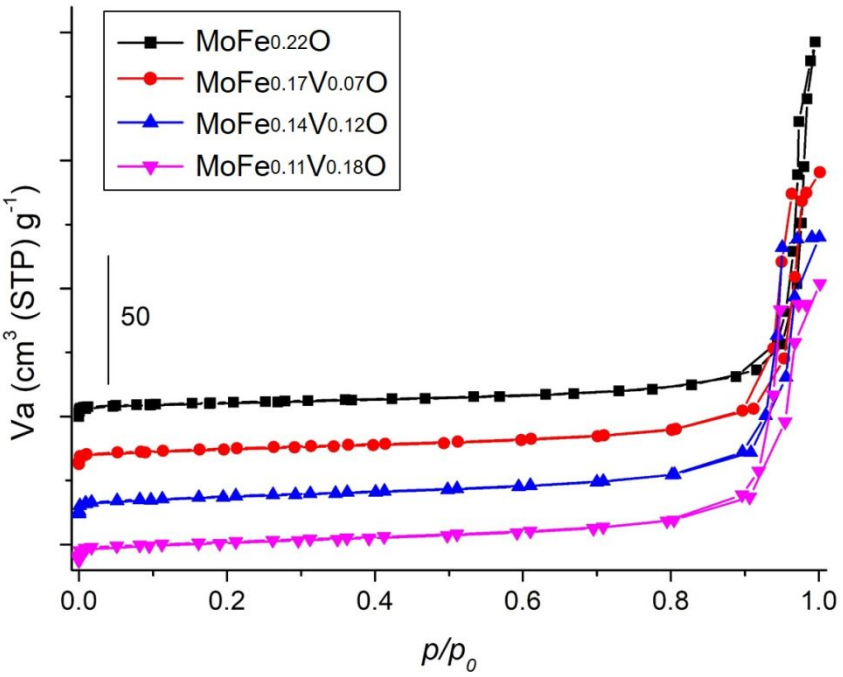

Figure S9. N_2 adsorption-desorption isotherms of the materials and BET surface area of **$MoFe_{0.22}O$** (20 m^2/g), **$MoFe_{0.17}V_{0.07}O$** (21 m^2/g), **$MoFe_{0.14}V_{0.12}O$** (24 m^2/g), and **$MoFe_{0.11}V_{0.18}O$** (26 m^2/g).

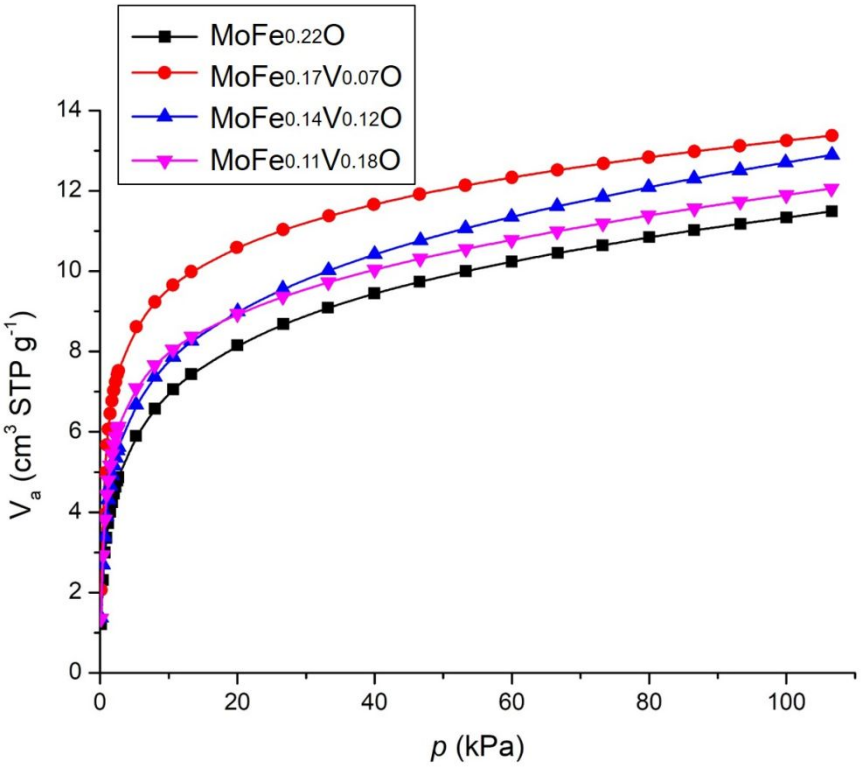

Figure S10. CO_2 adsorption isotherms of the materials.

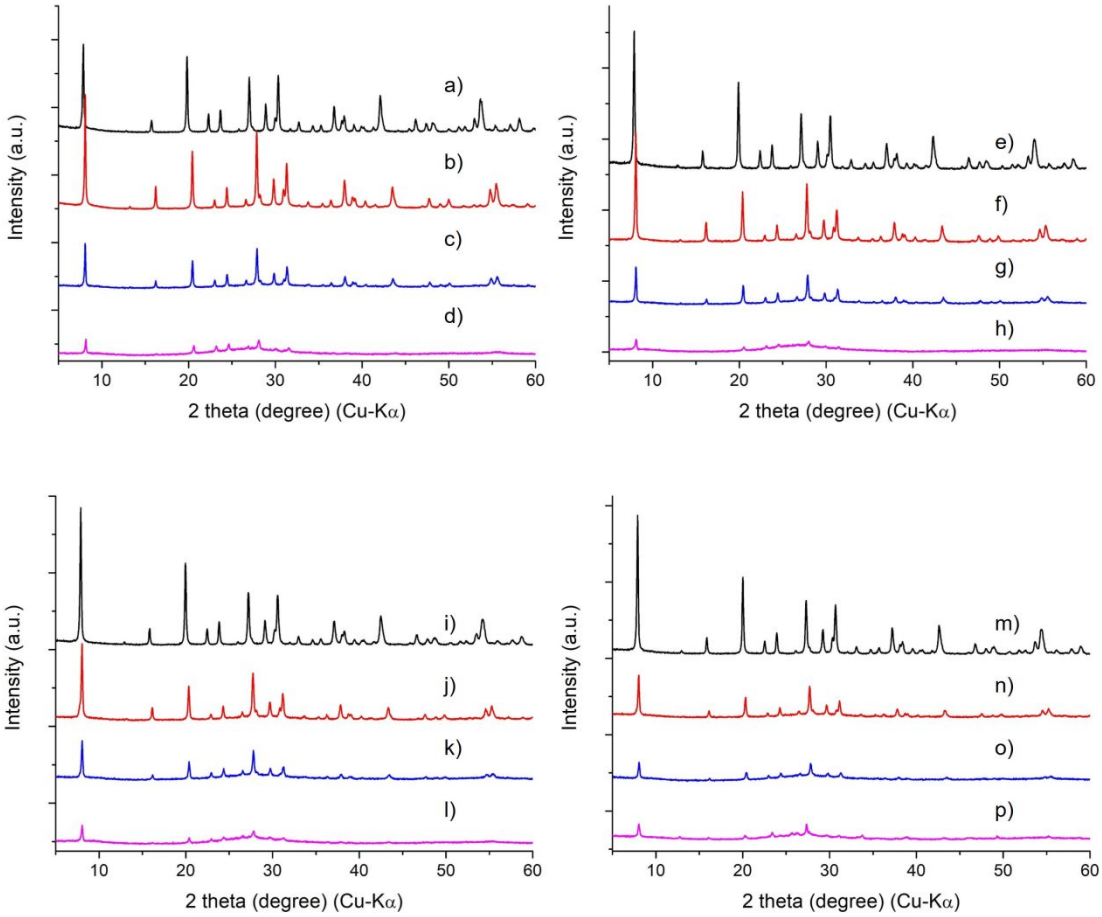

Figure S11. XRD patterns of **$MoFe_{0.22}O$**, a) as-synthesized material, b) calcined at 150 °C, c) 200 °C, and d) 250 °C; XRD patterns of **$MoFe_{0.17}V_{0.07}O$**, e) as-synthesized material, f) calcined at 150 °C, g) 200 °C, and h) 250 °C; XRD patterns of **$MoFe_{0.14}V_{0.12}O$**, i) as-synthesized material, j) calcined at 150 °C, k) 200 °C, and l) 250 °C; XRD patterns of **$MoFe_{0.11}V_{0.18}O$**, m) as-synthesized material, n) calcined at 150 °C, o) 200 °C, and p) 250 °C.

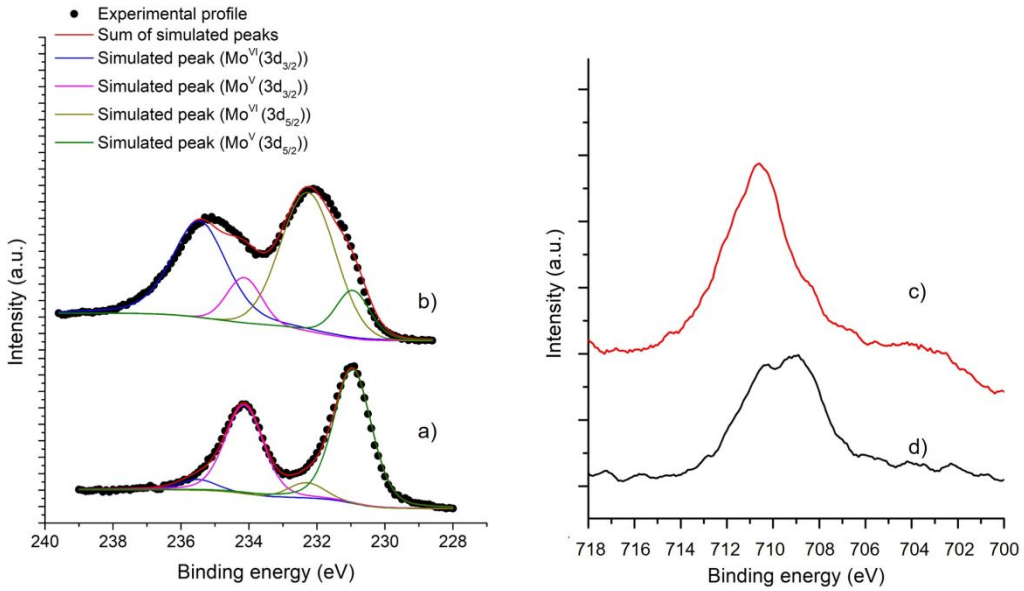

Figure S12. XPS profiles of Mo in a) **$MoFe_{0.22}O$** and b) **$MoFe_{0.22}O$** after O_2 adsorption at room temperature and Fe in c) **$MoFe_{0.22}O$** and d) **$MoFe_{0.22}O$** after O_2 adsorption at room temperature.

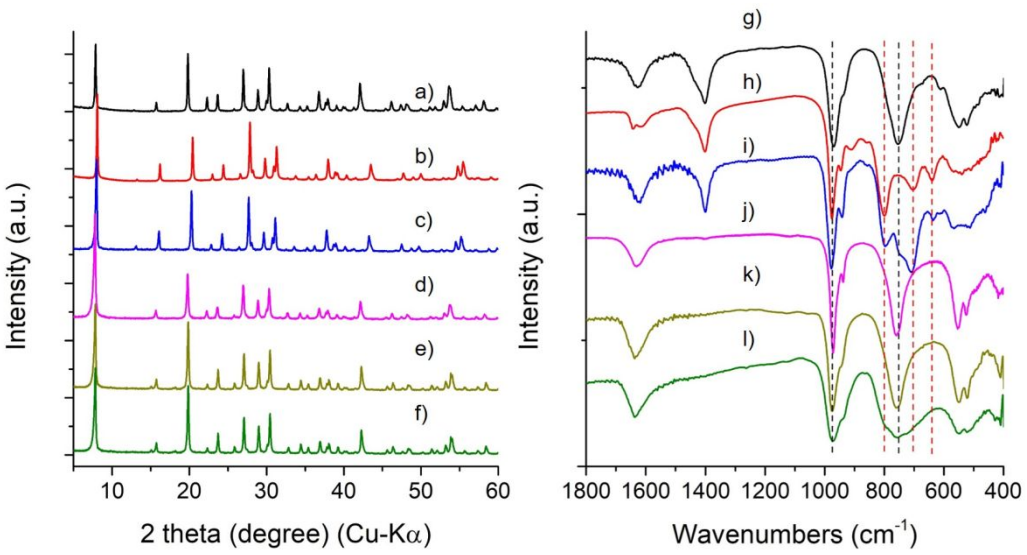

Figure S13. XRD patterns of a) **$MoFe_{0.22}O$**, b) **$MoFe_{0.22}OAC150$**, c) **$MoFe_{0.22}O$** after O_2 adsorption, d) **MoZnO**, e) **FeMoZnO**, and f) **FeMoZnO** after O_2 adsorption; FTIR spectra of g) **$MoFe_{0.22}O$**, h) **$MoFe_{0.22}OAC150$**, i) **$MoFe_{0.22}O$** after O_2 adsorption, j) **MoZnO**, k) **FeMoZnO**, and l) **FeMoZnO** after O_2 adsorption

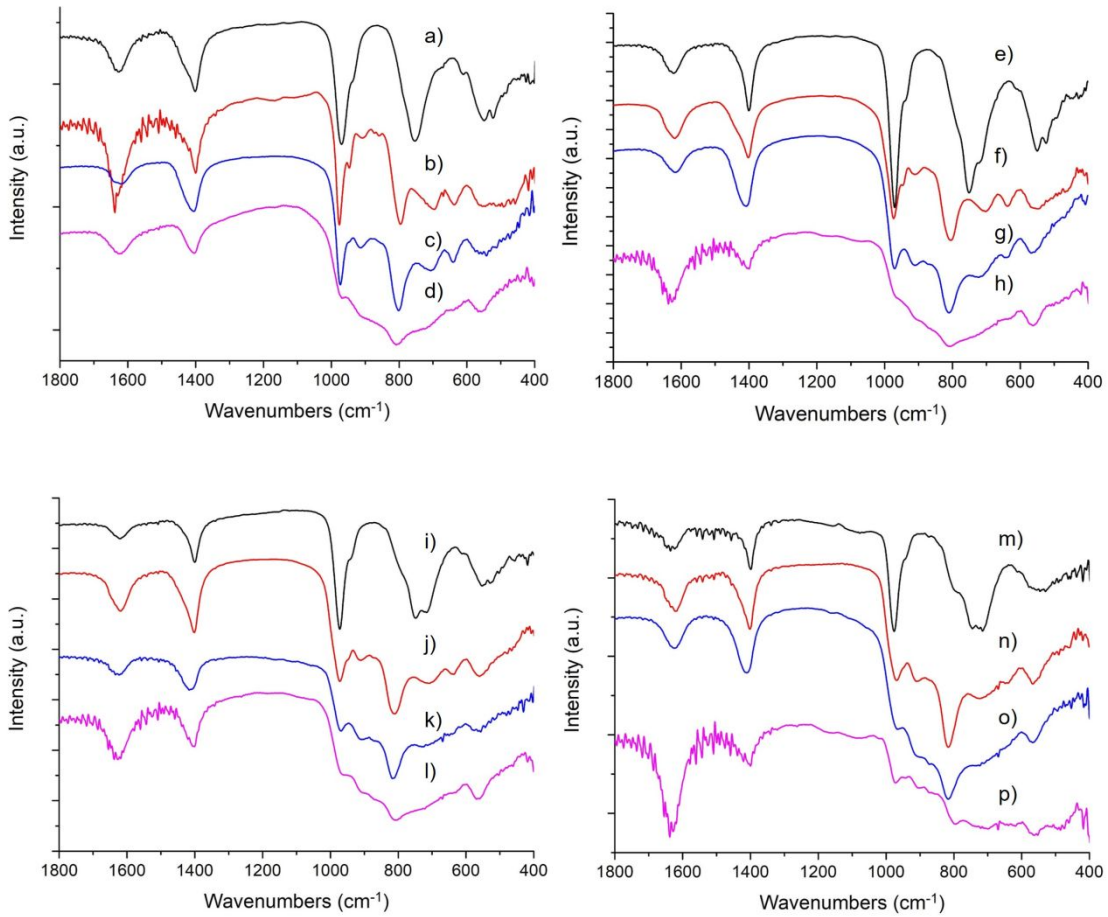

Figure S14. FTIR spectra of **$MoFe_{0.22}O$**, a) as-synthesized material, b) calcined at 150 °C, c) 200 °C, and d) 250 °C; FTIR spectra of **$MoFe_{0.17}V_{0.07}O$**, e) as-synthesized material, f) calcined at 150 °C, g) 200 °C, and h) 250 °C; FTIR spectra of **$MoFe_{0.14}V_{0.12}O$**, i) as-synthesized material, j) calcined at 150 °C, k) 200 °C, and l) 250 °C; FTIR spectra of **$MoFe_{0.11}V_{0.18}O$**, m) as-synthesized material, n) calcined at 150 °C, o) 200 °C, and p) 250 °C.

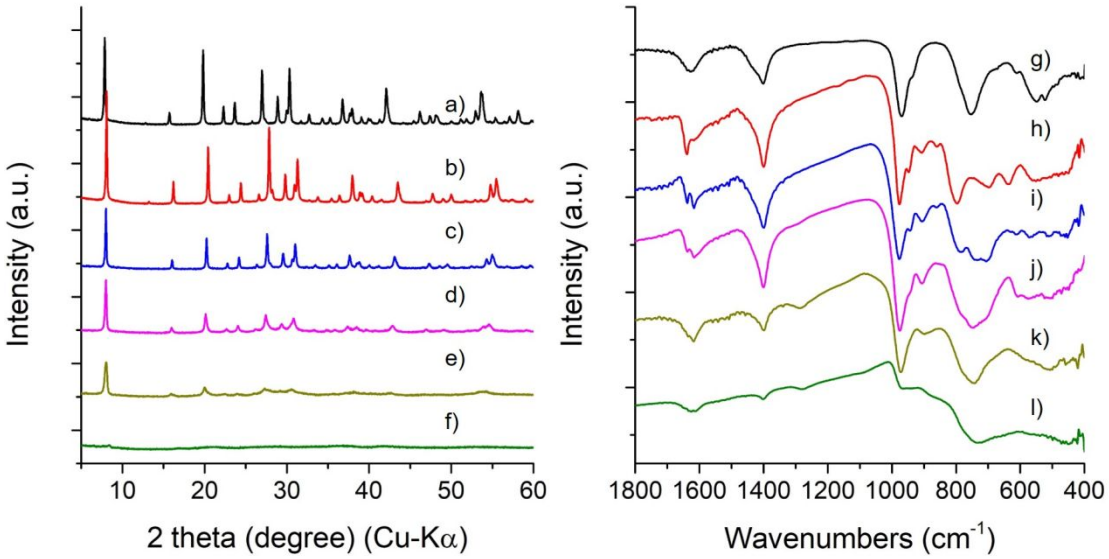

Figure S15. XRD pattern of a) **$MoFe_{0.22}O$**, b) **$MoFe_{0.22}$OAC150**, c) **$MoFe_{0.22}$OAC150HC150**, d) **$MoFe_{0.22}$OAC150HC200**, e) **$MoFe_{0.22}$OAC150HC250**, and f) **$MoFe_{0.22}$OAC150HC300**; FTIR spectra of g) **$MoFe_{0.22}O$**, h) **$MoFe_{0.22}$OAC150**, i) **$MoFe_{0.22}$OAC150HC150**, j) **$MoFe_{0.22}$OAC150HC200**, k) **$MoFe_{0.22}$OAC150HC250**, and l) **$MoFe_{0.22}$OAC150HC300**

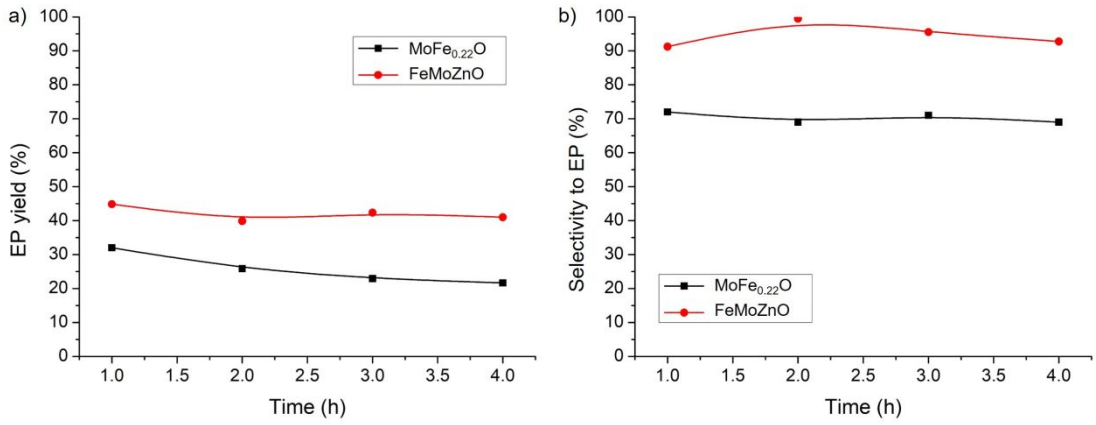

Figure S 16. The catalytic activity of the materials for EL oxidation to form EP, a) the EP yield and b) the selectivity to EP, Reaction conditions: Air 20 mL/min (N_2 15.6 mL/min, O_2 4.2 mL/min), EL 1.95 mL/min, catalyst 0.5 g, and temperature 200 ^oC.

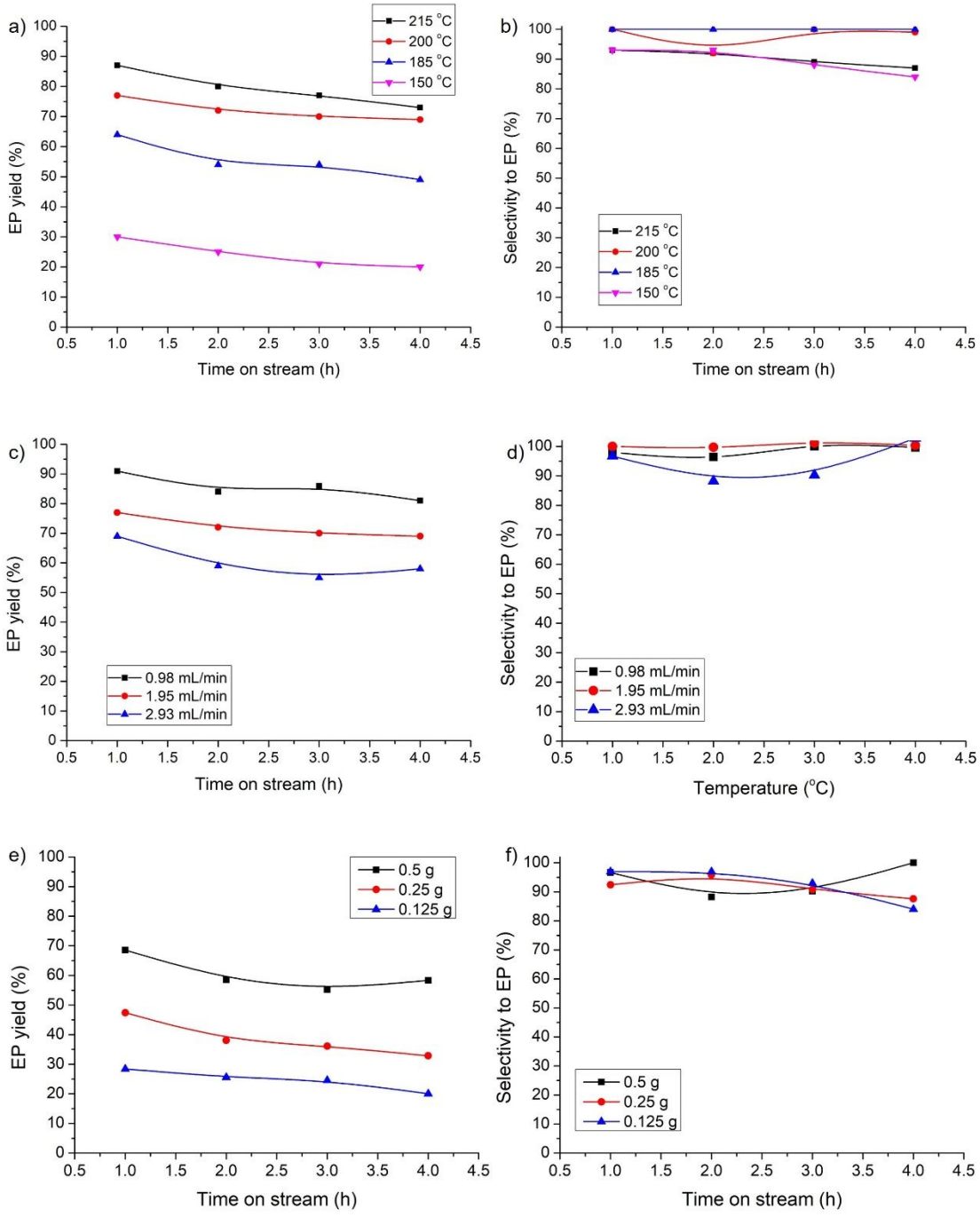

Figure S17. The catalytic activity of **$MoFe_{0.14}V_{0.12}O$** for EL oxidation. Temperature effect a) the EP yield and b) the selectivity to EP, Reaction conditions: Air 20 mL/min (N_2 15.6 mL/min, O_2 4.2 mL/min), EL 1.95 mL/min, catalyst 0.5 g. The EL flow rate effect c) the EP yield and d) the selectivity to EP, Reaction conditions: Air 20 mL/min (N_2 15.6 mL/min, O_2 4.2 mL/min), catalyst 0.5 g, and temperature 200 °C. Catalyst amount effect e) the EP yield and f) the selectivity to EP, Reaction conditions: Air 20 mL/min (N_2 15.6 mL/min, O_2 4.2 mL/min), EL 1.95 mL/min, and temperature 200 °C.

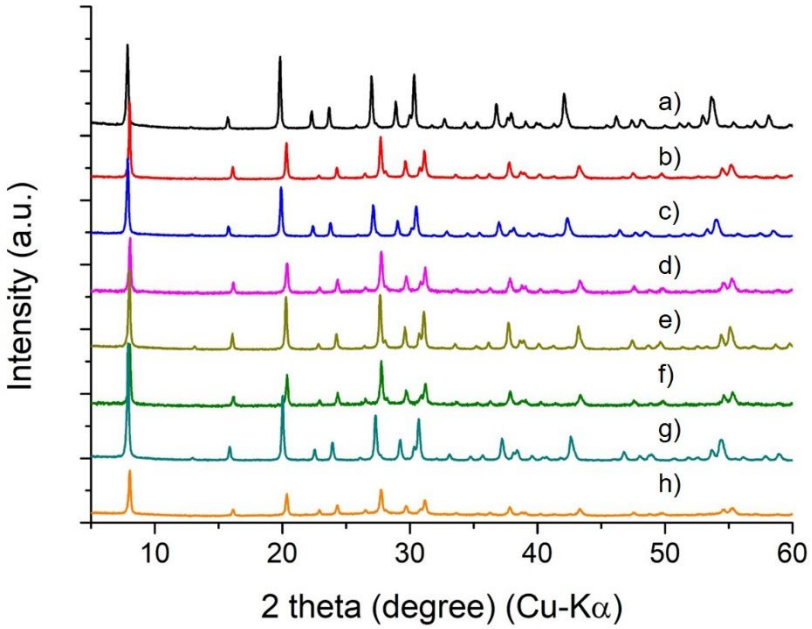

Figure S18. XRD patterns of a) **$MoFe_{0.22}O$**, b) **$MoFe_{0.22}O$** after the reaction, c) **$MoFe_{0.17}V_{0.07}O$** d) **$MoFe_{0.17}V_{0.07}O$** after the reaction e) **$MoFe_{0.14}V_{0.12}O$** f) **$MoFe_{0.14}V_{0.12}O$** after the reaction, g) **$MoFe_{0.11}V_{0.18}O$**, and h) **$MoFe_{0.11}V_{0.18}O$** after the reaction.

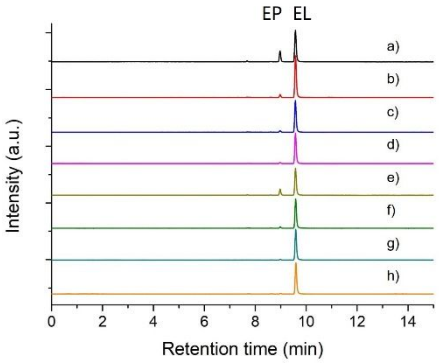

Figure S19. GC-FID profiles of **$MoFe_{0.22}O$** during the reaction a) 20 min, b) 40 min, c) 60 min, and d) 80 min, during the reaction after O_2 regeneration for e) 20 min, f) 40 min, g) 60 min, and h) 80 min.

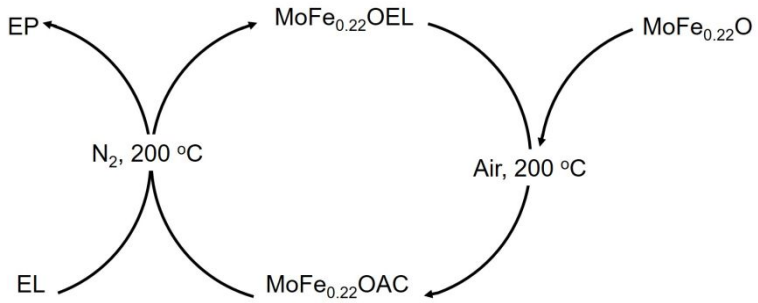

Figure S20. Catalytic cycle of EL oxidation catalyzed by **$MoFe_{0.22}O$**.

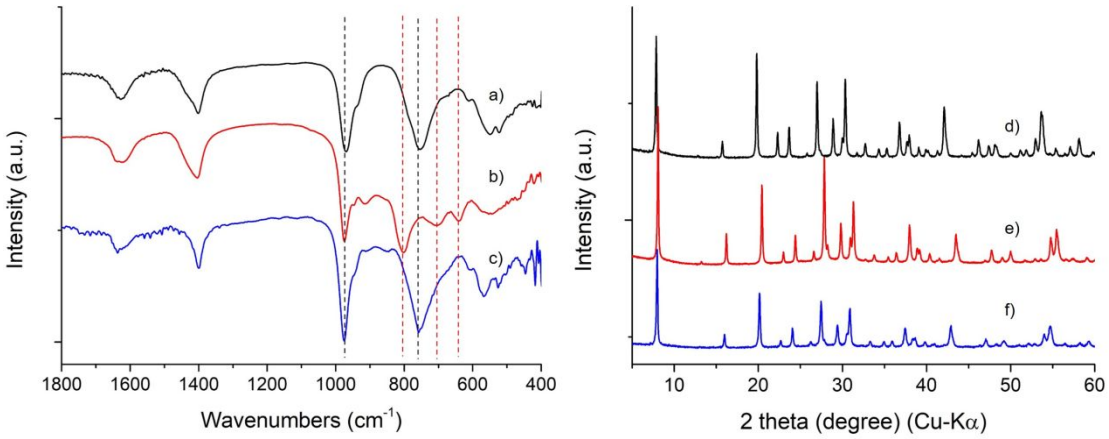

Figure S21. FTIR spectra of a) **MoFe$_{0.22}$O**, b) **MoFe$_{0.22}$OAC**, and c) **MoFe$_{0.22}$OEL**; XRD patterns of d) **MoFe$_{0.22}$O**, e) **MoFe$_{0.22}$OAC**, and f) **MoFe$_{0.22}$OEL**.

Table S1. The result of **$MoFe_{0.22}O$** from the charge-flipping algorithm.

Entry	X	Y	Z	Peak intensity	Assignement
1	0.0466	0.0465	0.8285	3.17	Mo
2	0.1249	0.125	0.1249	2.83	Fe
3	0.0705	0.0702	0.9297	1.06	O (framework)
4	0	0	0	1.09	-
5	0.0591	0.1649	0.8353	0.73	O (framework)
6	-0.0044	0.1759	0.3245	0.65	O (framework)
7	0.0321	0.0321	0.0321	0.48	O (framework)
8	0	0	0.3705	0.43	O (cation)
9	0.0797	0.0816	0.0819	0.35	-
10	0.1255	0.1251	0.6254	0.46	O (cation)
11	0.0348	0.1759	0.0348	0.48	O (framework)
12	0.0449	0.0996	0.5982	0.35	O (cation)
13	0.0844	0.113	0.5385	0.34	O (cation)

Table S2. Crystallographic information of **$MoFe_{0.22}O$** from Rietveld analysis.

	$MoFe_{0.22}O$	**$MoFe_{0.22}OAC150$**	1 h	3 h	9 h	20 h
crystal system	Cubic	Cubic	Cubic	Cubic	Cubic	Cubic
space group	$Fd\bar{3}m$	$Fd\bar{3}m$	$Fd\bar{3}m$	$Fd\bar{3}m$	$Fd\bar{3}m$	$Fd\bar{3}m$
$a = b = c$ (Å)	19.54983	18.95204	19.23206	19.28150	19.46821	19.52896
$\alpha = \beta = \gamma$ (degree)	90	90	90	90	90	90
R_{wp}	7.67%	5.93%	7.29%	7.04%	7.56%	7.05%
$R_{wp(w/o\ bck)}$	18.78%	17.98%	20.31%	19.03%	18.81%	18.08%
R_p	5.85%	4.16%	5.43%	5.26%	5.60%	5.19%
pattern parameter						
peak shape						
function	Pseudo-Voigt	Pseudo-Voigt	Pseudo-Voigt	Pseudo-Voigt	Pseudo-Voigt	Pseudo-Voigt
FWHM	U = 0.00653,	U = 0.18922,	U = 0.12498	U = 0.12801	U = 0.05785	U = 0.08110
	V = 0.05019,	V = -0.01907,	V = 0.01951	V = 0.00446	V = 0.01960	V = 0.02739
	W = 0.01668	W = 0.01767	W = 0.01493	W = 0.01639	W = 0.01713	W = 0.01683
profile parameter	N_A = 0.96780,	N_A = 0.92998	N_A = 0.96214	N_A = 0.92036	N_A = 0.86942	N_A = 0.89605
	N_B = -0.00482	N_B = 0.00057	N_B = -0.00105	N_B = 0.00018	N_B = 0.00032	N_B = -0.00052
line shift						
instrument geometry	Bragg-Brentano	Bragg-Brentano	Bragg-Brentano	Bragg-Brentano	Bragg-Brentano	Bragg-Brentano
zero point	-0.10418	-0.05893	-0.01208	-0.07949	-0.32749	-0.24150
shift#1	0.14685	0.06349	0.00266	0.07070	-0.32749	0.24503
shift#2	-0.04973	0.01305	0.02727	0.02955	0.02804	-0.00417
correction:						
method	Berar-Baldinozzi	Berar-Baldinozzi	Berar-Baldinozzi	Berar-Baldinozzi	Berar-Baldinozzi	Berar-Baldinozzi
parameter	P1 = 0.00972	P1 = -0.03194,	P1 = 0.03862	P1 = 0.01033	P1 = -0.02764	P1 = -0.01808
	P2 = -0.01184	P2 = 0.04226,	P2 = 0.04170	P2 = 0.01589	P2 = -0.06211	P2 = -0.07968
	P3 = -0.11934	P3 = -0.03368,	P3 = -0.16119	P3 = -0.09873	P3 = -0.02179	P3 = -0.04409
	P4 = 0.01216	P4 = -0.09764	P4 = -0.09761	P4 = -0.04528	P4 = 0.10907	P4 = 0.14470
background coefficients	Polynomial = 20	Polynomial = 20	Polynomial = 20	Polynomial = 20	Polynomial = 20	Polynomial = 20
Preferred orientation	March-Dollase	March-Dollase	March-Dollase	March-Dollase	March-Dollase	March-Dollase
	1.24623	1.21580	0.78138	1.33377	1.32219	1.31383

Table S3. Atom position, temperature factor, and occupancy of **$MoFe_{0.22}O$**.

	X	Y	Z	U_{iso}	Occupancy
O1	0.32014	0.52657	-0.38497	0.06	0.52
O2	0.02316	0.12931	0.07453	0.06	0.73
O3	-0.02306	0.21677	0.21677	0.06	0.24
Mo4	0.0771	0.45376	0.1729	0.005	1
O5	0.07237	0.35523	0.17763	0.06	1
O6	0.06856	0.46915	0.28085	0.06	1
Fe7	0.25	0.5	0.25	0.02	1
O8	0.09585	0.65415	0.09585	0.06	1
O9	0.06868	0.45882	0.06868	0.06	1

Table S4. Atom position, temperature factor, and occupancy of **$MoFe_{0.22}$OAC150**.

	X	Y	Z	U_{iso}	Occupancy
O1	0.22885	0.57244	-0.28198	0.06	0.23
O2	0.10762	0.08592	0.16408	0.06	0.08
Mo3	0.07071	0.44908	0.17929	0.005	1
O4	0.06463	0.3514	0.18537	0.06	1
O5	0.05957	0.46546	0.28454	0.06	1
Fe6	0.25	0.5	0.25	0.02	1
O7	0.08407	0.66593	0.08407	0.06	1
O8	0.06985	0.45886	0.06985	0.06	1
O9	0.11348	0.25159	0.11348	0.06	0.79

Table S5. Atom position, temperature factor, and occupancy of **MoFe$_{0.22}$OAC150** reduced for 1 h.

	X	Y	Z	U_{iso}	Occupancy
O1	0.20745	0.54255	-0.25247	0.06	0.27
O2	0.00493	0.24507	0.09704	0.06	0.24
Mo3	0.0745	0.45012	0.1755	0.005	1
O4	0.065	0.35012	0.185	0.06	1
O5	0.06272	0.46547	0.28453	0.06	1
Fe6	0.25	0.5	0.25	0.02	1
O7	0.08825	0.66175	0.08825	0.06	1
O8	0.06479	0.45801	0.06479	0.06	1
O9	0.13963	0.22874	0.13963	0.06	0.82

Table S6. Atom position, temperature factor, and occupancy of **$MoFe_{0.22}$OAC150** reduced for 3h.

	X	Y	Z	U_{iso}	Occupancy
O1	0.25278	0.45709	-0.20709	0.06	0.27
O2	0.49385	-0.09085	0.25615	0.06	0.25
Mo3	0.07503	0.4505	0.17497	0.005	1
O4	0.06506	0.35259	0.18494	0.06	1
O5	0.06729	0.46806	0.28194	0.06	1
Fe6	0.25	0.5	0.25	0.02	1
O7	0.08905	0.66095	0.08905	0.06	1
O8	0.06504	0.45826	0.06504	0.06	1
O9	0.1079	0.22983	0.1079	0.06	0.8

Table S7. Atom position, temperature factor, and occupancy of **$MoFe_{0.22}$OAC150** reduced for 9h.

	X	Y	Z	U_{iso}	Occupancy
O1	0.20761	0.54239	-0.25148	0.06	0.29
O2	0.00639	0.2436	0.08914	0.06	0.25
Mo3	0.07635	0.45114	0.17365	0.005	1
O4	0.06525	0.35363	0.18475	0.06	1
O5	0.06811	0.46894	0.28106	0.06	1
Fe6	0.25	0.5	0.25	0.02	1
O7	0.08765	0.66235	0.08765	0.06	1
O8	0.06579	0.46031	0.06579	0.06	1
O9	0.14277	0.22776	0.14277	0.06	0.76

Table S8. Atom position, temperature factor, and occupancy of **$MoFe_{0.22}$OAC150** reduced for 20 h.

	X	Y	Z	U_{iso}	Occupancy
O1	0.23208	0.4396	-0.38404	0.06	0.35
O2	0.02253	0.13073	0.07515	0.06	0.6
O3	0.03509	0.25912	0.21492	0.06	0.19
Mo4	0.07709	0.45249	0.17291	0.005	1
O5	0.07237	0.35523	0.17763	0.06	1
O6	0.0715	0.46931	0.28069	0.06	1
Fe7	0.25	0.5	0.25	0.02	1
O8	0.09304	0.65696	0.09304	0.06	1
O9	0.06744	0.4601	0.06744	0.06	1

Table S9. Comparison of the present catalyst with the previous reported catalysts for gas phase EL oxidation.

Catalyst	Temperature (°C)	Other conditions	Conv.(%)	Sel.(%)	ref
$MoFe_{0.14}V_{0.12}O$	200	Catalyst 0.5 g, Air 20 mL/min, EL 1.95 mL/min	77	99	This work
$MoFe_{0.14}V_{0.12}O$	200	Catalyst 0.5 g, Air 20 mL/min, EL 0.98 mL/min	91	98	This work
V_2O_5/TiO_2	200	Catalyst: 1g, Air 2.25 L/h (molar ratio of $EL/O_2 = 2.3$)	78	62	[32]
V_2O_5/CeO_2	200	Catalyst: 1g, Air 2.25 L/h (molar ratio of $EL/O_2 = 2.3$)	1	32.2	[32]
V_2O_5/MgO	200	Catalyst: 1g, Air 2.25 L/h (molar ratio of $EL/O_2 = 2.3$)	15.9	0.5	[32]
V_2O_5/ZrO_2	200	Catalyst: 1g, Air 2.25 L/h (molar ratio of $EL/O_2 = 2.3$)	28.5	43.9	[32]
V_2O_5/Al_2O_3	200	Catalyst: 1g, Air 2.25 L/h (molar ratio of $EL/O_2 = 2.3$)	35.6	36.7	[32]
MoVNbO	210	Catalyst: 1g, P_{EL} = 7 kPa, P_{O_2} = 40 kPa,	ca. 90	ca. 92	[33]
$MoVNbO_x/TiO_2$	190	P_{EL}= 20 kPa, P_{O_2}= 20 kPa, P_{He}= 61 kPa, space velocity=12 h^{-1}	78	86	[34]
$CoTeMoO_6$	200	5% EL, 30% O_2 , space velocity 3600 h^{-1}	ca. 30	ca. 90	[35]
Te_2MoO_7	250	5% EL, 30% O_2 , space velocity 3600 h^{-1}	ca. 20	ca. 90	[35]
$MnTeMoO_6$	250	5% EL, 30% O_2 , space velocity 3600 h^{-1}	ca. 30	ca. 90	[35]
$ZnTeMoO_6$	250	5% EL, 30% O_2 , space velocity 3600 h^{-1}	ca. 15	ca. 90	[35]

Reference:

(1) Shiju, R. N.; Technol, C. S.; Ccyj, D. O. I. Understanding the Oxidative Dehydrogenation of Ethyl Lactate to Ethyl Pyruvate over Vanadia/Titania Catalysts. *Catal. Sci. Technol.* **2018**, *8*, 3737–3747.

(2) Zhang, L.; Wang, R.; Song, L.; Zhao, X.; Fan, Q.; Li, H.; Yu, Q.; Li, X. Aerobic Oxidative Dehydrogenation of Ethyl Lactate Over Reduced $MoVNbO_x$ Catalysts. *Catal. Letters* **2019**, *149*, 840–850.

(3) Zhao, X.; Zhang, C.; Xu, C.; Li, H.; Huang, H.; Song, L.; Li, X. Kinetics Study for the Oxidative Dehydrogenation of Ethyl Lactate to Ethyl Pyruvate over $MoVNbO_x$ Based Catalysts. *Chem. Eng. J.* **2016**, *296*, 217–224.

(4) Hayashi, H.; Sugiyama, S.; Kokawa, N.; Koto, K. Additive Telluromolybdates as Catalyst for Vapor-Phase Selective Oxidation of Ethyl Lactate to Pyruvate. *Appl. Surf. Sci.* **1997**, *122*, 378–381.